A Robust System for Earth Current Measurements Related to Atmospheric Electric Fields

Ernst D. Schmitter
University of Applied Sciences Osnabrueck
Faculty of Engineering and Computer Sciences
49076 Osnabrueck, Germany
Email: e.d.schmitter@hs-osnabrueck.de

***Abstract*—**Monitoring geomagnetic and geoelectric field variations is of great importance for geophysical studies. We present a novel system for the measurement of shallow running earth currents on short distances (tens of meters) that proves as a reliable and inexpensive sensor for the surface Earth electric field as part of the global electric circuit. It is well suited to study electrified clouds, aerosol concentrations as well as averaged diurnal and seasonal surface electric field variations. It is less fragile than mechanical field mills, less prone to noise and more robust with regard to static discharges compared to electrometer (charge amplifier) devices and is therefore well suited for continuous unattended operation.

***Keywords*—**Earth currents, Earth electric field, signal processing

I. Introduction

We present a system sensing the surface earth electric field using earth ground as a conductor. It is well known, that geomagnetic field variations are of great importance to geophysics ([1], [2], [3]), but also the surface atmospheric electric field is an important parameter for example indicating aerosol concentration as well as cloud electrification [4], [5] on a diurnal time base. Seasonal variations of the averaged surface electric field are discussed to be related to climate change and solar activity, [6], [7]. A common instrument to measure the surface electric field is the field mill. It works by exposing an electrode plate to the electrostatic field and measuring it using a mechanical shutter rotating in front of the plate. Field mills can do very precise measurements, however they are quite expensive if a rugged outdoor device is needed. Other methods use different electrode geometries that are exposed to the electric field and are coupled to an electrometer (charge amplifier) to read the accumulated charge, [8]. Such devices however are very sensitive to static discharges and all electrodes directly exposed to the surface electric field suffer from local disturbances, especially wind drafts carrying along dust clouds.

We base our measurement approach on the observation that there is a closed current circuit between the lower ionosphere and earth ground forming the global electric circuit, fig. 1. The vertical current density j, assumed as constant during fair weather conditions (about $2 \cdot 10^{-12} Am^{-2}$, [7]), is related to conductivity σ and vertical electric field E at height h through (cp. [9])

$$j = \sigma(h)E(h) \tag{1}$$

Atmospheric conductivity increases with height because of the growing ionization effect of cosmic rays, which means that the electric field decreases accordingly, having its maximum near the ground (about 130 V/m with fair weather). Conductivity within the surface layer can be subject to strong local variations caused by cloud electrification but also air pollution (aerosols reducing the number of current contributing ions by attachment to particles). The atmospheric current has to enter the earth ground to close the circuit. Our earth electrode system is set up to record the horizontal circuit balancing currents. Another source for earth currents are geomagnetic storms, [10]. Solar activity causes variations of the geomagnetic field inducing electric fields in the earth ground which in turn generate earth currents. Such geomagnetically induced currents (GICs) according to Maxwell's equations are proportional to the time derivative of the geomagnetic field. During the observation campaign reported in this paper we did not record any geomagnetic signatures, the atmospheric electric field effects dominates our results. With regard to the mid latitude (52N) and the short measurement distance ($L = 36m$) this is comprehensible because geomagnetic effects strongly increase polewards. In the next chapter we explain the mode of operation of the measurement system. Afterwards we discuss single event records as well as diurnal and seasonal signal behavior.

II. The Measurement System

Fig. 2 shows the layout for our earth current measurement system. Two identical orthogonally oriented measurement systems each with two electrodes at a distance of $L = 36m$ are in operation: one in west-east direction and another one north-south oriented. Zinc-plated steel tent pegs of 0.5 m length driven into the ground serve as electrodes. The symmetric high pass input of the system not only rejects common mode noise but also suppresses the DC offset generated by the electrode-ground electro-chemical interfaces. The time constant is $T = RC = 1000s$. Analyzing the circuit (fig. 2) yields $V_{ext} = 2V_C + V_{mon}$, where V_C is the voltage drop at capacitor C. With $C\dot{V}_C = I$, where I is the current through C and $2RI = V_{mon}$ (assuming ideal circuit symmetry and infinitely high input impedance for the instrumentation amplifier) we get

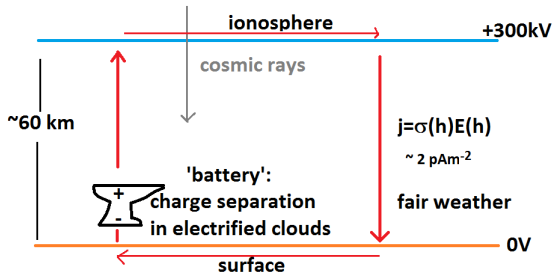

Fig. 1. The global electric circuit. Cosmic rays and very near to the surface also ground radioactivity generate positive and (consecutively by electron attachment) negative ions that render the atmosphere weakly conductive. Conductivity increases exponentially with height. The vertical electric field decreases accordingly. Charge separation in thunderclouds and electrified shower clouds are the batteries keeping up a voltage difference of about 300 kV between the lower ionosphere and the earth ground. A fair weather current density of about $2pAm^{-2}$ is continually discharging the global electric system.

$$\dot{V}_{ext} = \dot{V}_{mon} + \frac{1}{T} V_{mon} \tag{2}$$

and

$$V_{ext} = V_{mon} + \frac{1}{T} \int V_{mon} dt \tag{3}$$

For a conductor with a total resistance R_E, length L and cross section A consisting of a material of conductivity σ we get:

$$R_E = \frac{1}{\sigma} \frac{L}{A} \tag{4}$$

Typical values for ground conductivity are: $\sigma = 0.05..3 \cdot 10^{-2} S/m$ for earth ground depending on its dryness, $\sigma \cong 5 \cdot 10^{-2} S/m$ for sweet water and $\sigma \cong 5\ S/m$ for sea water. (1 Siemens $= 1\Omega^{-1}$). Measurement of R_E is done by applying an AC signal (to avoid electro-chemical DC offset problems) of known voltage (5V RMS, $90Hz$, injected at the points marked as red in fig. 2) and measuring the current flowing. Several weeks after installing the electrodes the resistance in both directions settled to $R_E = 960..1040\Omega$. With an estimated value of $\sigma \cong 10^{-2} S/m$ for rather wet ground and $L = 36m$ we get from equ. 4 $A \cong 3.6m^2 \cong 1.9m \times 1.9m$ as a rough estimate for the earth cross section contributing to the conduction between the two electrodes. As expected we record near surface currents. The wires running from the electrodes to the recording device are isolated and shallowly buried in the ground, so that they are not exposed to the earth electric field.

III. Results

All recordings discussed in this paper have been carried out at a mid latitude site (52.1N, 8.5E) between July 2013 and March 2014 in a rural environment. The measurement legs are

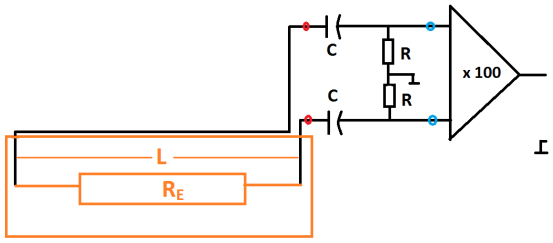

Fig. 2. Earth current monitoring schematic. Between the red dots: V_{ext}; between the blue dots: V_{mon}. Both voltages are related by equations 2 and 3. $C = 100\mu F$, $R = 10M\Omega$, $T = RC = 1000s$; $L = 36m$; $R_E \cong 1000\Omega$; Data acquisition period: 1s. An instrumentation amplifier increases the voltage level by a factor of 100 for convenient recording. All results in this paper are discussed in terms of V_{ext}/L.

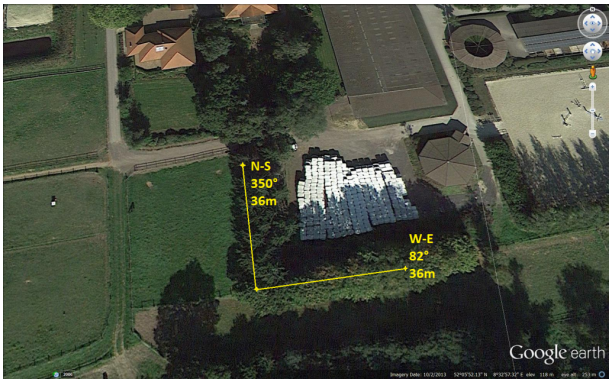

Fig. 3. Site at 52.1N8.5E with the Earth current monitoring lines in W-E and N-S directions along the edges of a group of trees. The recording device with two identical circuits according to fig. 2 is located near to the electrode which is common to both lines (lower left).

situated at the edges of a group of trees, fig. 3. In this way they are shielded from the direct effect of rain or snow precipitation. Results are discussed in terms of V_{ext}/L (volt per meter), cp. equ. 3, with $L = 36m$. The earth current is related to V_{ext} by Ohm's law: $I_E = V_{ext}/R_E$ (neglecting the resistance of the wires to the electrodes). Regular measurements of the resistance R_E confirmed that its value did not change significantly during dry or wet weather conditions. Signal amplitudes on the W-E path typically proved to be about 3 times larger than with the N-S path despite $R_E \cong 1k\Omega$ is nearly equal in both directions. We now present some results of our campaign with regard to single events and afterwards with regard to the averaged diurnal and seasonal characteristics.

A. Single Events

On the late afternoon of the 29th of July 2013 a thunderstorm passed over the acquisition area from west to east, fig. 4. Its signature is clearly more developed with the N-S path orthogonal to the storm moving direction (note however the different scales of W-E and N-S channels). Times of sunrise and sunset are marked with red (rise) and black (set) vertical

lines. The inlay shows the zoomed data between 12 and 17 UT. The first drop is correlated with an advancing thunderstorm cloud without near lightning, so acting by its electrification on the surface electric field. The events around 15 UT are related to near lightning strokes. The drop around 2 UT in the night from the 30th to the 31st of July is caused by an west-east moving electrified cloud system with showers, also more prominent with the N-S recording path.

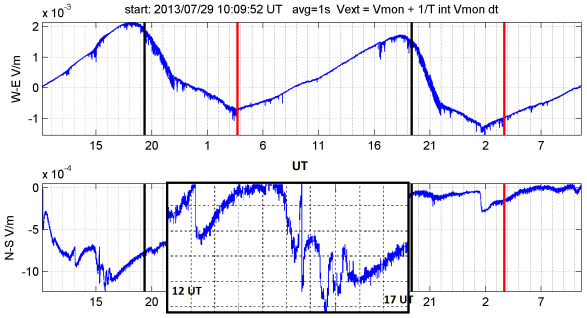

Fig. 4. Thunderstorm passing overhead the data acquisition area around 15 UT 29th July 2013. The disturbance is clearly more pronounced with the N-S channel than with the W-E channel. The inlay shows the zoomed data between 12 and 17 UT. The thunderstorm moved from W to E. Black lines: sunset, red lines: sunrise.

On the 5th of Dec. continuing to the 6th of Dec. 2013 the very strong storm front Xaver passed the acquisition area from west to east, fig. 5. Air pressure (4th panel from top in the figure) decreases the whole day (5th Dec.) and reaches a minimum around 16 UT. The main storm front passed the data acquisition area between 14 and 17 UT indicated by the sharp signal drops (where the minima coincide with sunset) on both channels (note the different scales). Only for about 20 minutes around 17 UT there was a rain shower. Thunderstorm cells have been observed within the storm front but did not pass directly overhead (at least 20 km distance to the nearest lightnings). So the main synchronous drops on both channels are not related to showers but to electric field changes caused by cloud electrification and surface near aerosols driven by the strong winds.

Fig. 6 shows the signal course during a dry fair weather situation, where the dips in the afternoon around 18 UT (the black line indicates local sunset time) are caused by wind gusts carrying aerosols that catch ions which in this way are lost for the vertical current, so conductivity is decreased and the electric field value is increased.

B. Diurnal and Seasonal Averages

More than a century ago Wilson, [11] identified thunderstorms and electrified shower clouds as the batteries driving the global electric circuit, fig. 1. He based his hypothesis on the similarity between the diurnal variation of thunderstorm days in universal time and the Carnegie curve of the electric field, named after the geophysical survey vessel of the Carnegie Institution of Washington on which the original measurements demonstrating the universal time variation of the surface electric field have been done, fig. 11, [12], [13], [14].

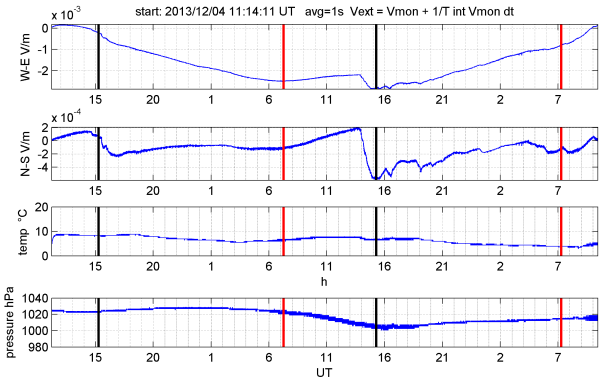

Fig. 5. Storm front Xaver, 5th/6th Dec. 2013. Air pressure (4th panel from top) decreases the whole day (5th Dec.), reaching its minimum around 16 UT. The main storm front passed the data acquisition area between 14 and 17 UT indicated by the sharp signal drops on both channels (note the different scales). Only for about 20 minutes around 17 UT there was a rain shower. Thunderstorm cells have been observed within the storm front but did not pass directly overhead (at least 20 km distance to nearest lightnings).

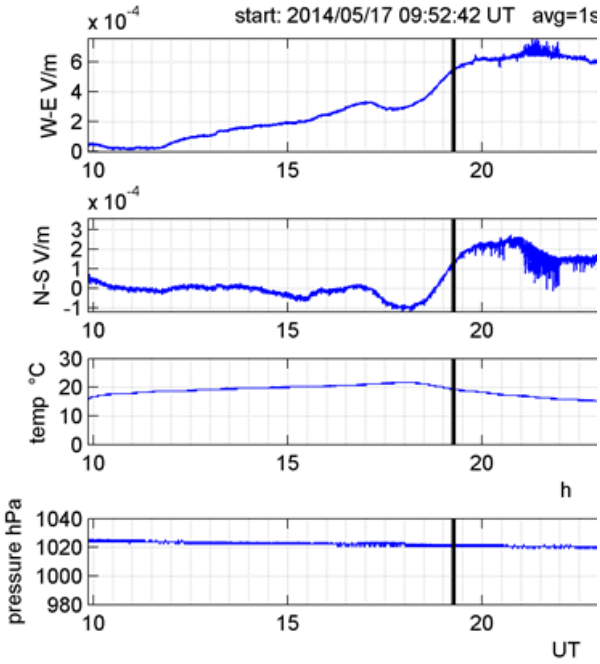

Fig. 6. Signal dips (upper two panels) around 18 UT during a dry fair weather situation (the black line indicates local sunset time). Wind gusts carry aerosols catching ions which in this way are lost for the vertical current, so conductivity is decreased.

Fig. 7 shows diurnal signal averages in both channels for August, September, October 2013 (ASO), fig. 8 for November, December 2013, January 2014 (NDC) and fig. 9 for February, March, April 2014 (FMA). In all cases a 5-term Fourier-series (including a constant term, equ. 5) is fitted to the data yielding a near perfect fit, especially with the W-E channel. This implies that the superposition of 4 periods (24, 12, 8 and 6 hours) together with a constant offset explains the diurnal course of the averaged V_{ext}/L signals nearly completely.

$$E_{avg}(t) = \sum_{i=0}^{i=4} a_i \ sin(i\frac{2\pi t}{24} + b_i) \quad (5)$$

Also displayed in the panels are the Carnegie-E-field-curves for the 3 months periods in question. These curves represent harmonic fits to the original Carnegie data. The parameters are tabulated in [12]. In our plots they are vertically scaled for a best fit to our data. We see quite good concordance with the Carnegie curve during ASO (northern late summer-autumn) with the W-E channel and during NDJ as well as FMA (northern winter and spring) with both channels. The N-S channel during ASO shows larger deviations. This might be due to the fact that the N-S channel is very sensitive to the frequent autumn time front systems moving from west to east leaving only few undisturbed days in that period. With regard to the seasonal behavior the ASO amplitudes with both channels are larger by a factor of 2 compared to the NDJ period.

A closer inspection of our data during NDJ and FMA shows a simple periodic structure with an early minimum near 8 UT (NDJ), 6 UT (FMA) and a late maximum near 16 UT (NDJ), 17 UT (FMA) in both channels. During ASO the situation is more complicated: the W-E channel has a minimum near 4 UT and a maximum near 19 UT. Both extrema are shifted by about 1.5 hours with the N-S channel. Also between the early minimum and late maximum additional structure appears. For comparison the Carnegie curves exhibit a minimum near 3 UT and maxima between 15-20 UT (two maxima in FMA) . Further recordings are in progress to allow calculating averages for coming seasons and reveal more details. Especially the following question asks for an answer: which part of the characteristics observed is locked to local time (sunrise and sunset) and which part is globally caused (global distribution of electrified clouds) and locked to universal time.

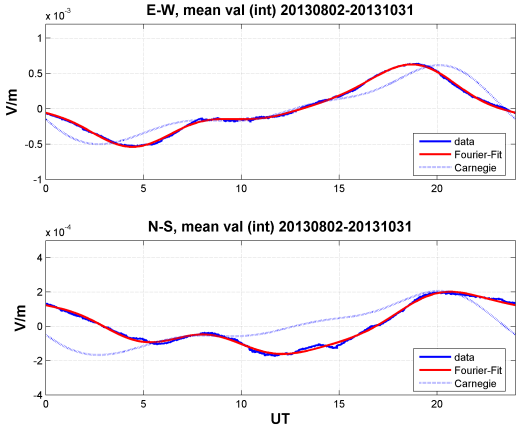

Fig. 7. August-September-October (ASO) seasonal averages with Fourier-fits and ASO Carnegie curves, see text.

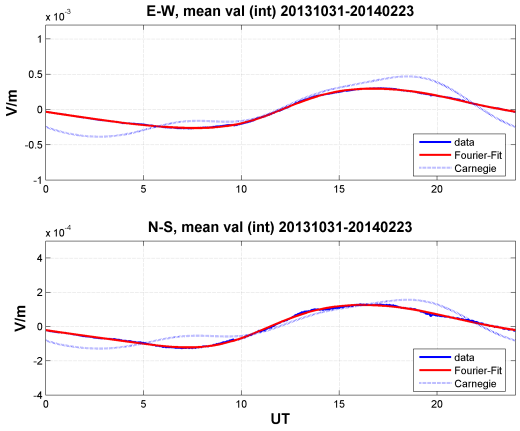

Fig. 8. November-December-January (NDJ) seasonal averages with Fourier-fits and NDJ Carnegie curves, see text.

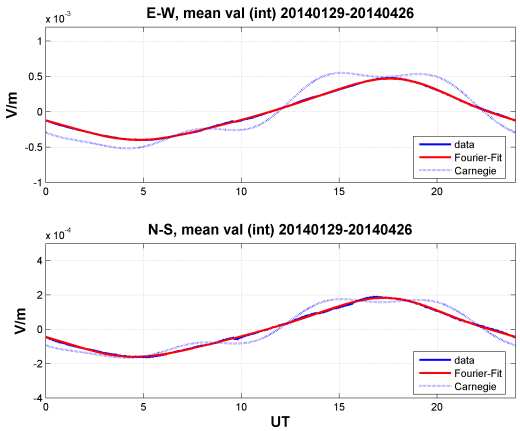

Fig. 9. February-March-April (FMA) seasonal averages with Fourier-fits and FMA Carnegie curves, see text.

IV. Conclusion

We have presented a novel measurement system that can be used as a reliable sensor for the earth surface electric field. Its effectiveness has been shown with regard to the detection of electrified clouds and aerosols, but also by displaying diurnal and seasonal characteristics related to the global electric field variation, figs. 10, 11. It avoids some disadvantages of common systems resulting from their direct exposition to the electric field, especially local noise and failure from static discharges with electrometer systems. Having no mechanical components and no openly accessible electrodes a continuous and unattended operation is easily possible. Our monitoring is continued to gain further insight into qualitative and quantitative aspects of single events (especially with regard to discriminate cloud electrification and aerosol caused signatures) and to get a better understanding of the diurnal and seasonal characteristics with regard to local and global drivers.

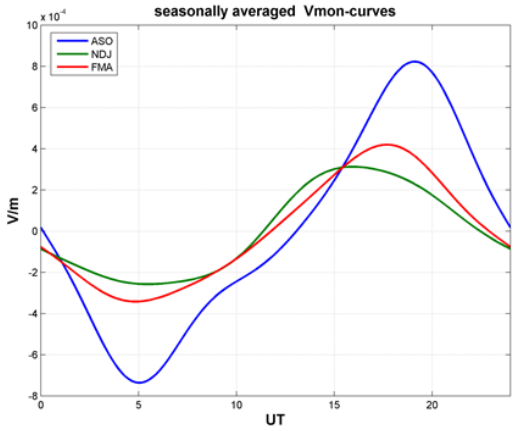

Fig. 10. Seasonal Fourier-fits to our data, cp. figs. 7, 8, 9, E-W channel. The morning minima and evening maxima clearly correlate with the Carnegie electric field data, cp. fig. 11. The amplitudes of the ASO and NDJ seasonal data however anti-correlate.

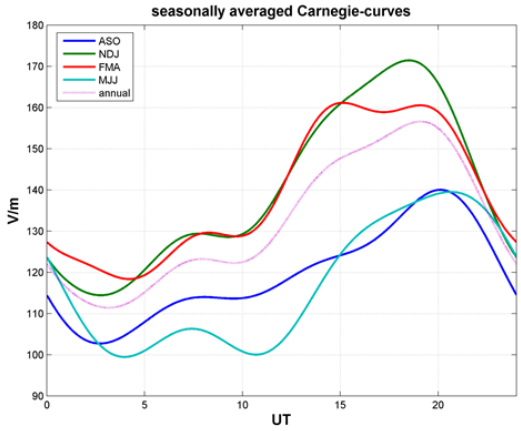

Fig. 11. Seasonal Carnegie surface electric field curves, adapted from [12].

REFERENCES

[1] Schmitter, E.D., Analysing and Classifying Geomagnetic Activity Data in a Noisy Environment. Proceedings of the 11th WSEAS Int. Conf. on Systems (CSCC07), Agios Nicolaos, Crete, Greece, July 23-25, 2007, pp. 154-157

[2] Schmitter, E.D., Modelling Geomagnetic Activity Data. WSEAS Transactions on Signal Processing, Volume 4, pp. 6-11, 2008

[3] Schmitter, E.D., Low Frequency Radiation Processes Around the Earth - Phenomena and Numerical Modeling, The 4th IASME / WSEAS International Conference on Geology and Seismology (GES '10), Cambridge, UK, February 23-25, 2010

[4] Bennett, A.J., Harrison, R.G., Variability in surface atmospheric electric field measurements, Journal of Physics, Conference Series 142, 012046, 2008, doi:10.1088/1742-6596/142/1/012046

[5] Williams E.R., Heckman, S.J., The local diurnal variation of cloud electrification and the global diurnal variation of negative charge on the Earth, Journal of Geophysical Research , 98, D3, 5221-5234, 1993

[6] Harrison, R.G., The global atmospheric electrical circuit and climate, Surv. Geophys., vol. 25, 441-484, 2004

[7] Rycroft, M.J., Israelsson, S., Price, C., The global atmospheric electric circuit, solar activity and climate change. Journal of Atmospheric and Solar-Terrestrial Physics, 62, 15631576, 2000

[8] Bennett, A.J., Harrison, R.G., Surface measurement system for the atmospheric electrical vertical conduction current density, with displacement current density correction, Journal of Atmospheric and Solar-Terrestrial Physics 70, 1373 1381, 2008

[9] Rycroft, M.J., Harrison, R.G. Nicoll, K.A., Mareev, E.A., An overview of Earths global electric circuit and atmospheric conductivity, Space Sci. Rev., vol. 137, 83-105, 2008

[10] Lehtinen, M., Pirjola, R., Currents produced in earthed conductor networks by geomagnetically-induced electric fields, Annales Geophysicae, 3, 4, 479-484, 1985

[11] Wilson, C. T. R., Atmospheric electricity, Nature, 68, 101104, 1903

[12] Harrison, R.G., The Carnegie Curve, Surv. Geophys., 34:209232, 2013, doi 10.1007/s10712-012-9210-2

[13] Liu, C., Williams, E.R., Zipser, E.J., Burns, G., Diurnal Variations of Global Thunderstorms and Electrified Shower Clouds and Their Contribution to the Global Electrical Circuit, Journal of the Atmospheric Sciences 67.2, 309-323, 2010

[14] Williams, E. R., The global electrical circuit: a review, Atmos. Res., vol. 91, 140-152, 2009